Lab on a Chip

Accepted Manuscript

ROYAL SOCIETY OF CHEMISTRY

www.rsc.org/loc

Clog-free Cell Filtration Using Resettable Cell Traps

William J. Beattie, Xi Qin, Lin Wang, and Hongshen Ma

A microfluidic cell separation mechanism created using constrictions with adjustable size that can selectively capture and release cells and thereby enabling high throughput size and deformability based cell separation without clogging.

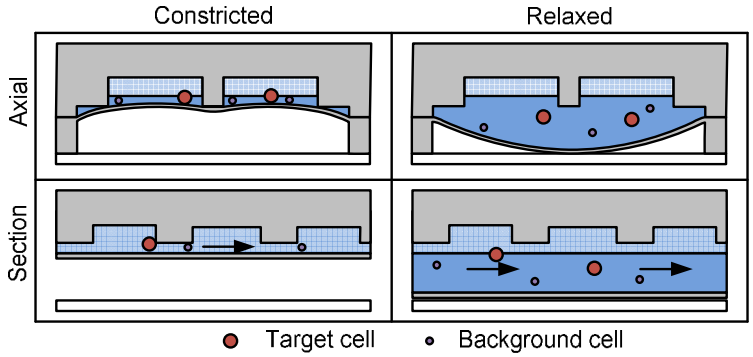

Clog-free Cell Filtration Using Resettable Cell Traps

William Beattie[a], Xi Qin[a], Lin Wang[a], and Hongshen Ma[a,b,c]

[a] *Department of Mechanical Engineering, University of British Columbia, 2054-6250 Applied Science Lane, Vancouver, BC, Canada V6T 1Z4*

[b] *Vancouver Prostate Centre, Vancouver General Hospital, Vancouver, BC, Canada*

[c] *Department of Urologic Science, University of British Columbia, Vancouver, BC, Canada*

Abstract

The separation of cells by filtration through microstructured constrictions is limited by clogging and adsorption, which reduce selectivity and prevent the extraction of separated cells. To address this key challenge, we developed a mechanism for simply and reliably adjusting the cross-section of a microfluidic channel to selectively capture cells based on a combination of size and deformability. After a brief holding period, trapped cells can then be released back into flow, and if necessary, extracted for subsequent analysis. Periodically clearing filter constrictions of separated cells greatly improves selectivity and throughput, and minimizes adsorption of cells to the filter microstructure. This mechanism is capable of discriminating cell-sized polystyrene microspheres with <1 µm resolution. Rare cancer cells doped into leukocytes can be enriched ~1800X with ~90% yield despite a significant overlap in size between these cell types. An important characteristic of this process is that contaminant leukocytes are captured by non-specific adsorption and not mechanical constraint, enabling repeated filtration to improve performance. The throughput of this mechanism is 900,000 cells per hour for 32 multiplexed microchannels, or ~1200,000 cells/cm^2·hour on a per area basis, which exceed existing micropore filtration mechanisms by a factor of 20.

Introduction

The separation of cells based on their physical properties is important in many biological and biomedical applications where known physical differences can be used to distinguish target and background cells. For example, circulating tumor cells (CTCs) are thought to be distinguishable from peripheral blood cells based on physical characteristics [**1**] [**2**], while biochemical cell surface markers used to isolate CTCs in current processes are thought to be unreliable [**3**] [**4**]. Furthermore, these cells have been observed to arrest in the microvasculature because of their larger size and limited deformability [**5**], suggesting that

there may be situations where separation based on physical properties may be an appropriate method for capturing these cells.

Current methods in label-free cell separation can be classified as flow-based fractionation or micropore filtration. Flow-based fractionation methods function by laterally displacing cells across streamlines in a flow field using mechanisms such as size exclusion near obstacles [**8**] [**9**] [**10**], inertial forces [**11**] [**12**], and attraction using an electric [**13**] [**14**] [**15**] [**16**] or gravitational fields [**17**]. These methods typically discriminate cells based on size, density, and electrical permittivity, which limit their specificity because of the significant overlap in these parameters across different cell types. Micropore filtration relies on the deformation of individual cells through micrometer scale constrictions to separate cells based on a combination of size and deformability [**18**] [**19**] [**20**] [**21**]. This approach can often be more specific because deformability varies considerably more than the parameters used in flow-based fractionation across phenotypes [**22**] [**23**] [**24**]. The suitability of traditional membrane-based micropore filters for cell separation, however, is limited by the ability to precisely control the force used to deform cells across the filter microstructure, as well as the difficulties associated with the localization and extraction of the separated cells for further processing [**21**].

Microfluidic technologies have the potential to overcome these limitations by using fluidic circuitry to precisely control the force applied to each cell as it deforms through a constriction [**22**], as well as to direct the flow of separated cells for subsequent processing. However, micropore filtration in microfluidic devices is inherently low-throughput due to the planar nature of photolithographic microfabrication. Specifically, since flow in a microfluidic device is constrained to a 2D plane, the micro-scale constrictions used for separation can only be parallelized as a linear (1D) array. Additionally, cells trapped in filter constrictions block subsequent cells from transiting through the constrictions, and the buildup of these trapped cells alters the hydrodynamic resistance of the filter in an unpredictable way. To ensure the reliable operation of filtration devices, the number of filter constrictions must vastly outnumber the number of cells that are likely to be captured by the filter, which further limits throughput per constriction.

A variety of microfluidic filtration devices have been developed that use pneumatic pressure to produce an adjustable orifice, the earliest of which is the sieve valve [**25**]. Such devices have been employed to separate microspheres from suspension [**25**] [**26**] [**27**] [**28**], chondrocytes from a suspension of digested tissue [**26**], erythrocytes and plasma from whole blood [**27**], Filtration devices with adjustable geometry are able to expand and purge captured cells from the filter area [**27**] [**26**] [**28**], and bacteria from

suspension [**28**], but are often limited to low flow rates and have not yet been demonstrated to separate nucleated cell phenotypes. Separating nucleated phenotypes by filtration is considerably more difficult than separating particles form suspension or non-nucleated cells from nucleated cells because nucleated cells possess relatively similar physical properties. For example, the deformability of human leukocytes differs from that of RT4 bladder cancer cells by a factor of 3-4 [**22**], while leukocytes and erythrocytes differ in deformability by a factor of 20-40 [**29**].

To overcome these difficulties, we developed a microfluidic cell separation device using a resettable microstructure with the ability to alternate between capturing target cells from a heterogeneous mixture and releasing them back into the flow channel. The microstructure has sufficient precision to resolve differences between nucleated cell phenotypes, and can capture and release cells repeatedly, thus greatly expanding the throughput per constriction without compromising its selectivity.

Design

Resettable Cell Trap Mechanism

The structure of the resettable cell trap mechanism is shown in Figure 1A. Similar to conventional membrane micro-valves [**30**], the cell trap consists of an upper flow channel for the sample that overlaps a lower fluid-filled control channel. The two channels are separated by a thin diaphragm of elastomeric material that can be deflected up or down by a pressure difference between the channels. Unlike conventional micro-valves, the ceiling of the flow channel is a textured surface featuring a series of recesses and a protruding center fin that functions as a mechanical stop to limit the travel of the diaphragm (Figure 1B). The ability of a cell to transit through this microstructure is controlled by the cross-sectional opening of the channel, which in turn is determined by the position of the diaphragm (Figure 1C). Given sufficient pressure in the control layer, the diaphragm will deflect upward into contact with the center fin of the flow channel, effectively bisecting the flow channel along its length. The change in stiffness of the diaphragm can be approximated using the slender beam equation, under which halving the diaphragm width increases its stiffness by a factor of 16 [**31**]. This abrupt change in stiffness allows the membrane to assume a consistent shape once sufficient pressure has been applied to create a contact with the center fin. Additional pressure only serves to fine-tune the size of the opening. Recesses lining the ceiling of the flow channel serve as storage compartments for captured cells to occupy so the cells do not completely occlude the channel, allowing other cells to pass without clogging. Once the recesses fill up with captured cells, the channel is purged to empty the recesses.

While the diaphragm can be deflected continuously, there are two diaphragm positions useful for cell separation (Figure 1C). If the pressure difference across the diaphragm, herein known as the trapping pressure, is positive, the diaphragm is deflected upwards and contacts the center fin. This diaphragm position decreases the cross-sectional opening of the flow channel, configuring the trap in the constricted state. If the trapping pressure is negative, the diaphragm is deflected downwards and configures the trap in the relaxed state. The cell trap dimensions are designed such that the constricted state allows transit of background cells but is sufficiently small to arrest target cells, while the relaxed state readily allows the transit of all cells. In early experiments we observed target cells being captured at the front of the constriction, while background cells were captured throughout the constriction. Accordingly, we modified our design to minimize the length of the constricted region while still allowing the full inflation of the trap.

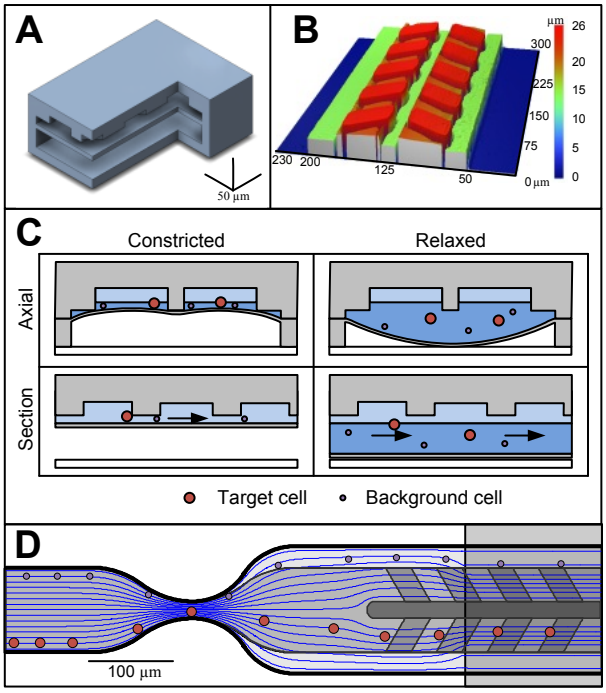

Figure 1. Structure and function of the resettable cell trap. A: Isometric cut-away view of the trap. The cell suspension flows through the upper channel. B: Profile of the mold for the flow channel as measured by a non-contact profilometer. C: Schematics of the cell trap in the constricted and relaxed states. Axial views show the deflection of the diaphragm floor under positive and negative trapping pressures. Section views show the effective channel height in both states. D: Top view of the hydrodynamic flow focuser upstream of the cell trap. Streamlines are superimposed in blue along with mock trajectories of large and small cells. Large cells will enter the cell trap area regardless of their initial lateral position upstream, while small cells may leak through the side and bypass the trap.

The cross-sectional shape of the constricted flow channel consists of two approximately rectangular channels flanked by two small triangular side channels (Figure 1C). While the rectangular channels have the recesses and controlled height that allow them to selectively capture target cells, the side channels do not. The side channels exist merely because the diaphragm is bound at the sides of the channel; they are not designed for separating cells. To prevent cells from entering these side channels, the mechanism features hydrodynamic flow focusers upstream of the cell trap to help center incoming cells (Figure 1D). These flow focusers, widely employed in microfluidic devices for processing cellular samples [**8**] [**9**], bring cells near the outer edges of the flow channel into physical contact with the channel walls, bumping the cells over to adjacent, more centered streamlines. In experiments, the larger and more rigid cancer cells did not enter these side channels after passing through the flow focuser.

A previous version of this mechanism was shown to impart different flow rates to different cell phenotypes to potentially enable chromatographic cell separation [**32**]. In this paper, we demonstrate a generalized method to use this mechanism for cell separation and subsequent extraction.

Cell Separation Device

The prototype cell separation device consists of 32 resettable cell traps in parallel and supporting microfluidic elements including bifurcation microchannels to evenly distribute cells into the parallelized cell traps [**33**]; inlet reservoirs for the cell sample and buffer; outlet reservoirs for the target cells and waste cells; and micro-valves to route flow between these components (Figure 2A). A serpentine channel between the cell traps and the outlet reservoirs provides a dominant hydrodynamic resistance that facilitates controlling the diaphragm deflection. Specifically, the hydrodynamic resistance of this element is more than 95% of the total device hydrodynamic resistance, such that the pressure drop between the sample inlet and cell trap is negligible. Consequently, the trapping pressure can be read off the pressure source gauges for the control and flow channel, thereby eliminating the need for on-chip pressure sensors to regulate the deflection of the trap diaphragm.

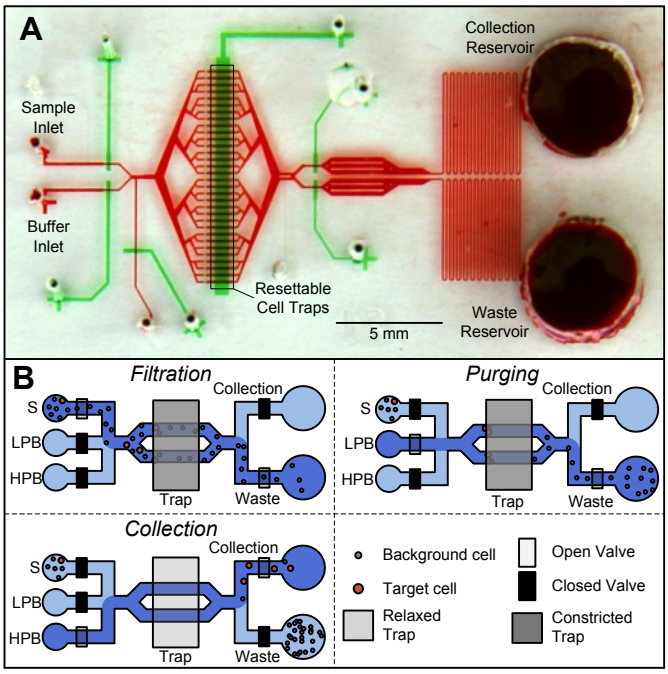

Figure 2. A: Photograph of the separation device with the flow and control channels are filled with red and green food coloring respectively. During the separation process, sample from the inlet is initially bifurcated into 32 parallelized cell traps. The resettable cell traps, formed at the intersections of the wide green bar and the parallelized flow channels, capture target cells from the flow. The filtered sample is then directed into the collection and waste outlets through serpentine hydrodynamic resistors. B: Schematic operational cycle of the cell separation device. Fluid is delivered from the sample inlet (S), low pressure buffer (LPB) or high pressure buffer (HPB) inlet and direct towards the waste or collection reservoir. The operational cycle consists of filtration, purging, and collection.

Operational Cycle

The cell separation device operates on a repeating three-step cycle of filtration, purging, and collection (Figure 2B). In the filtration step, the sample is flowed through a constricted cell trap. Target cells accumulate at the constricted trap while background cells flow through the trap and into the waste reservoir. Eventually the trap's recesses will fill with target cells and flow through the channel will be obstructed. In experiments we observed a dramatic decrease in the ability of leukocytes to transit through a trap once it held more than four trapped cells. Accordingly, the duration of the filtration step was limited such that a volume of sample containing on average no more than two target cells per trap was filtered before purging. In a separation application with unknown target cell concentration, a conservative estimate would be required to determine the proper period of filtration. In the purging step, the trap remains constricted while buffer fluid flows through the trap towards the waste outlet to remove background cells from trap area. This step typically requires 5-10 seconds. Finally, in the collection step, the cell trap is opened and the released target cells flow into the collection reservoir. The release flow is approximately 3-4 times as fast as the flow in filtration and purging. The increased

speed produces greater shear forces that remove cells that may have adhered to the walls of the cell traps [**34**]. A demonstration of the three-step cycle is provided in Video S1.

Results and Discussion

Separation Resolution

The ability of a particle to transit through the resettable cell trap is determined by the cross-sectional opening between the diaphragm and the channel ceiling. The size of this opening can be adjusted using the pressure difference between the flow and control channel to selectively capture particles greater than a certain diameter. To characterize the separation resolution of this mechanism, we measured the probability of capture for monodisperse microparticles as a function of the trapping pressure applied between the flow and control channels. The tested microparticles (Bangs Labs, Fishers, IN) included diameters of 6.4 ± 0.3 µm, 7.3 ± 0.4 µm, 9.5 ± 0.3 µm, and 10.1 ± 0.4 µm, selected to mimic the cross-sectional width of deformed cells. The results of these experiments are shown in Figure 3. For each particle size, the transition between no trapping and complete trapping occurs over 25-50 mbar of pressure (shown as shaded regions). More importantly, there is little to no overlap in the transition regions between different particle diameters, which indicate the resettable cell trap mechanism is capable of resolving particles with <1 µm resolution.

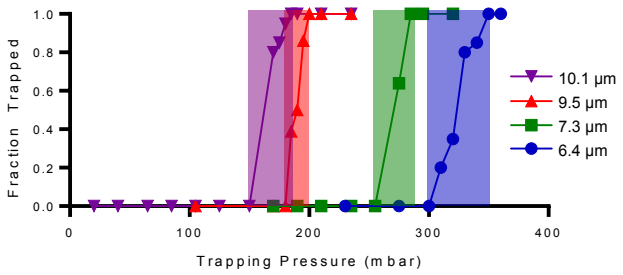

Figure 3. The probability of trapping microsphere as a function of pressure applied to the membrane. Smaller microspheres require smaller channel openings to be captured, and therefore require greater trapping pressure than larger microspheres. The range of trapping pressures for each particle size is shown as a colored block for each microsphere diameter, indicating the minimal overlap between sizes.

Cell Separation and Optimization

We evaluated the ability to separate different cell types using the resettable cell trap mechanism by separating cultured UM-UC13 bladder cancer cells (UC13) doped into a suspension of leukocytes. UC13

is a highly invasive phenotype that is EpCAM negative and therefore undetectable using established affinity-capture based techniques such as the Veridex CellSearch® system [**35**]. As detailed in following sections, we measured the physical properties of these cell types and found that UC13 are on average 5 µm greater in diameter and 5 to 10 times stiffer than leukocytes (Figure 5A & 5B). Importantly, these phenotypes have overlapping size distributions but significantly different deformability. The overlap in size distributions would therefore severely limit the effectiveness of separation mechanisms that discriminate solely based on size.

To optimize the resettable cell trap mechanism for the selective capture UC13 cells, we first determined the required membrane pressure by flowing UC13 cells through a single cell trap and adjusted the trapping pressure until 95% of incident cells were captured. The optimal membrane pressure was found to be 150 mbar. Next, we tested the separation of UC13 cells from leukocytes as a function of cell concentration in the suspending media, and the relative concentration of leukocytes to UC13. The key performance metrics are yield and enrichment. Yield refers to the fraction of target cells captured relative to the total processed population. Enrichment refers to the enhancement of the population of target cells relative to background cells in the outlet sample. We found the device to perform optimally at a concentration of ~$2 \cdot 10^6$ leukocytes/ml (*i.e.* whole blood diluted 1:1 using PBS) and a UC13-leukocyte doping ratio of ~1:1000.

To optimize the flow rate in the resettable cell trap structure, we tested the separation of UC13 cells from leukocytes from 5 different donors as a function of flow rate. As shown in Figure 4A, at a flow rate of <4 mm/s, the resettable cell trap device was able to consistently able to obtain a yield of 88-96%, as well as an enrichment value that increases with flow rate. For each data point, the measured result shown is the average of triplicate experiments. A key factor limiting enrichment is the non-specific adsorption of leukocytes to surfaces of the cell trap during the filtration phase. These adsorbed leukocytes are released with the UC13 cells during the collection phase, thereby limiting the purity of the output sample. As shown in Figure 4A, the enrichment of cancer cells relative to leukocytes improves with increasing flow speed because of the increased shear forces reduces non-specific adhesion of leukocytes [**34**]. The yield of UC13 cells is also not strongly dependent on flow rate at <4 mm/s. When the flow rate is raised to 6 mm/s, however, the yield of UC13 cells drops to ~70%. Additionally, some trapped UC13 cells show signs of morphology change where the previously round cells were observed to take on an elongated shape. Therefore, a flow rate of 4 mm/s is likely the practical limit for the resettable cell trap device to retain a reasonable yield and prevent cell damage

from high shear force. These results further confirm that contaminant leukocytes are caught in the filter because of non-specific adsorption rather than mechanical constraint as in the case of cancer cells.

Based on an optimized flow rate of 4 mm/s, we then investigated the repeatability of device performance across multiple donors and within each donor. The measured enrichment showed significant variability across different donors ranging from ~170 to ~870 across five donors (Figure 4B). This observation Is unsurprising since the properties of blood cells, specifically the non-specific adherence of leukocytes, can vary dramatically across humans, resulting in large variations in enrichment. When the device is tested using blood from the same donor, however, the measured enrichment and yield showed remarkable consistency (Figure 4C).

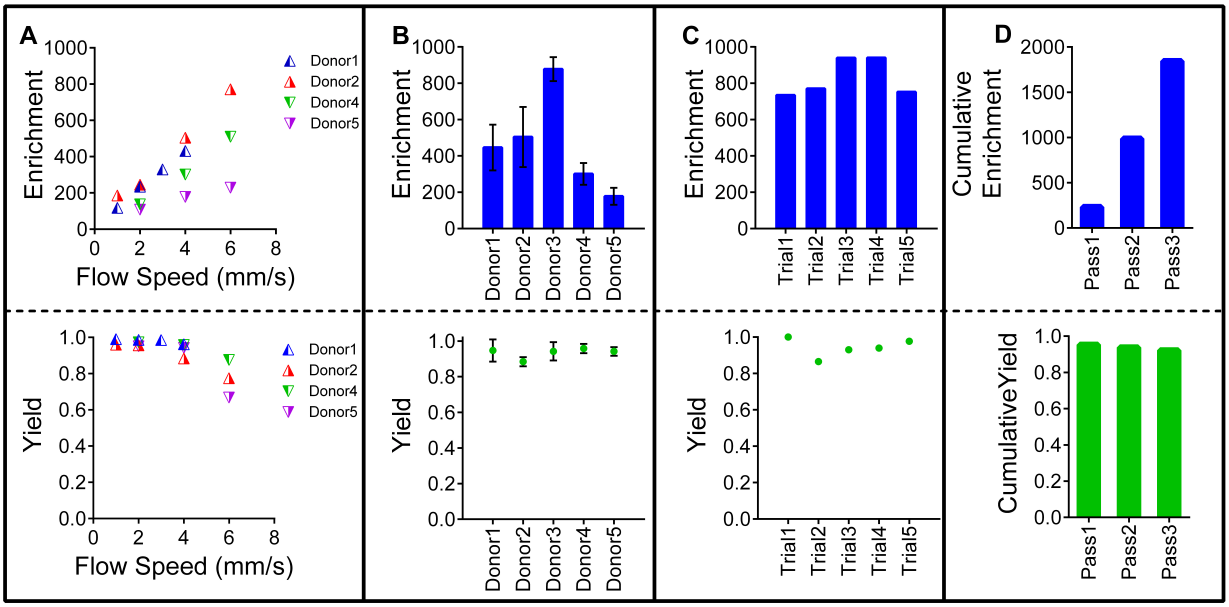

Figure 4. Performance of the resettable cell trap mechanism. A: Enrichment and yield of UC13 cells doped into whole blood as a function of flow rate from 5 different donors. Each data point is the average of triplicate experiments on the same sample. B: Enrichment of yield of the resettable cell trap mechanism across different donors tested at a flow rate of 4 mm/s. For each donor, 3-5 tests were performed. C: Enrichment and yield measured for the same donor at a flow rate of 4 mm/s. D: Enrichment and yield results from 3X serial filtrations showing improved enrichment and minimal degradation in yield.

Serial Enrichment

One of the key results of our initial cell separation experiments is the realization that while cancer cells are caught in the cell trap because of mechanical constraint, while leukocytes are caught because of non-specific adsorption. This result suggests that repeatedly filtering the sample through multiple traps could improve the level of target cell enrichment. To test this hypothesis, we processed a sample with a starting concentration of $2{\cdot}10^6$ leukocytes/ml and UC13 cells doped into leukocytes at a ratio of 1:1,000. After each pass through the device, the waste and collection outlets are imaged to count the number of leukocytes and UC13 in each. We then pipetted the contents of the collection outlet back into the sample inlet, emptied the waste reservoir, and repeated the separation process. As shown in Figure 4C, while the first filtration step provides the greatest individual enrichment of the ratio of UC13 relative to leukocytes, subsequent steps also provided substantial additional enrichment. The compounded effect of all three steps is an enrichment of 1,845, with significant improvement compared to the single step results described in the previous section. Importantly, loss of target cells occurred almost entirely in the first step, which means that 90% of the target cells were retained even after three re-filtration steps. These results validate the idea that leukocytes are captured in the microstructure because of non-specific adhesion rather than mechanical constraint, and suggest that the level of enrichment could be improved even further with more rounds of re-filtering. This capability is being integrated in future versions of this device for rare cell separation applications such as the isolation of CTCs.

Separation Based on Size and Deformability

Cell separation techniques that discriminate based on size alone are attractive because to their simplicity of operation and their high throughput. This approach, however, can be ineffective in applications where target and background cells are of similar size. As a filtration based mechanism, the resettable cell trap discriminates based on a combination of size and deformability and is likely to offer superior performance in these applications. To investigate this enhanced discrimination, we characterized the size and deformability of the target and background cell types (Figure 5A and 5B). Given the overlapping size distributions of UC13 and leukocytes, separation based on size alone would result in significantly heterogeneous separation result. For example, selecting all the cells in the mixture greater than 20 µm in diameter would eliminate all leukocytes, but would also eliminate the vast majority of UC13. Selecting all cells greater than 10 µm would ensure all UC13 were retained, but a significant fraction of leukocytes would contaminate the output. Figure 5C shows the receiver-operator curve of the maximum possible discrimination using size-only based separation. The additional

discrimination provided by deformability based separation enables the performance of resettable cell trap mechanism to greatly exceed this limit.

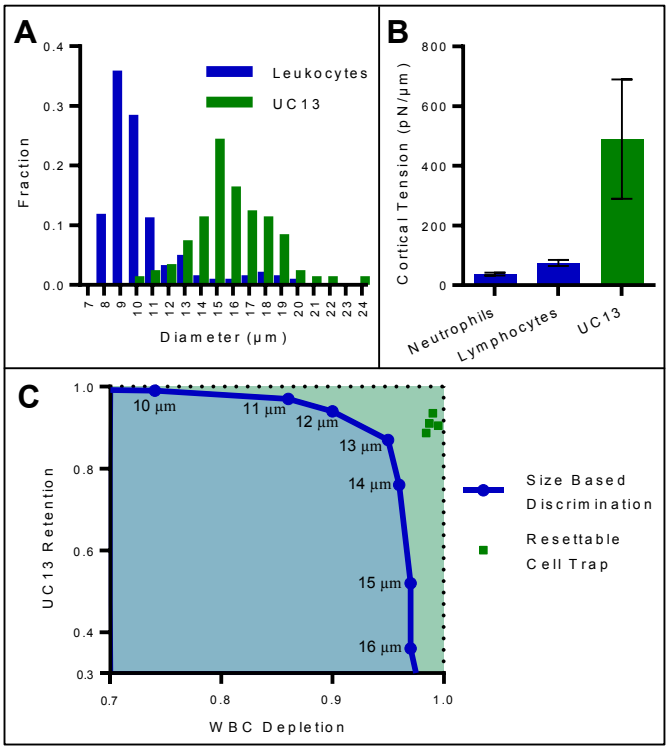

Figure 5. A: Size distribution of UC13 and leukocytes (N≈100 for each population). There is substantial size overlap between the two phenotypes in the 11-15 µm range. B: Deformability of neutrophils, lymphocytes, and UC13 as measured by microfluidic micropipette aspiration [22]. C: Theoretical ROC for size based cell separation showing target cell yield and background cell depletion at different threshold diameters. The performance of the resettable cell trap mechanism shows significant improvement over the theoretical maximum for size-based separation.

Importance of the Anti-clogging Mechanism

The effectiveness of micropore filtration is limited by clogging, whereby the presence of cells captured by the filter alters the hydrodynamic resistance of the filter in an unpredictable manner and resulting in reduced selectivity. This problem can be mitigated by increasing the number of micropores such that the filtered cells occupy only a small fraction of the pores. However, doing so increases the device footprint and therefore reduces the throughput per unit area. The resettable cell trap mechanism avoids clogging problems altogether by periodically emptying the cell traps to enable sustained and reliable operation. To demonstrate the importance of this capability, Figure 6 shows the accumulation of cells in two traps: one is kept in the constricted state and never emptied, while the other is periodically purged and reset. UC13, captured primarily through mechanical constraint, accumulate at the first point of constriction near the front of the trap. Leukocytes, captured through a combination of adsorption and mechanical

constraint, begin to accumulate throughout the length of the trap's constriction. The non-resettable filter is fouled after just two minutes of operation. In contrast, periodically resetting the cell traps keeps the filter microstructure clear of cells, allowing the filtration process to continue indefinitely without decreasing the selectivity of the trap. Additionally, the ability to temporarily capture and release target cells reduces the amount of time these cells are pressed against the filter microstructures, thereby reducing adsorption and allowing target cells to be released and collected. The separated cells can then be analyzed by downstream microfluidic elements or extracted by pipetting. Other micropore filtration techniques do not accommodate the release of captured cells [**20**] [**21**], necessitating additional complexity for subsequent characterization of these cells.

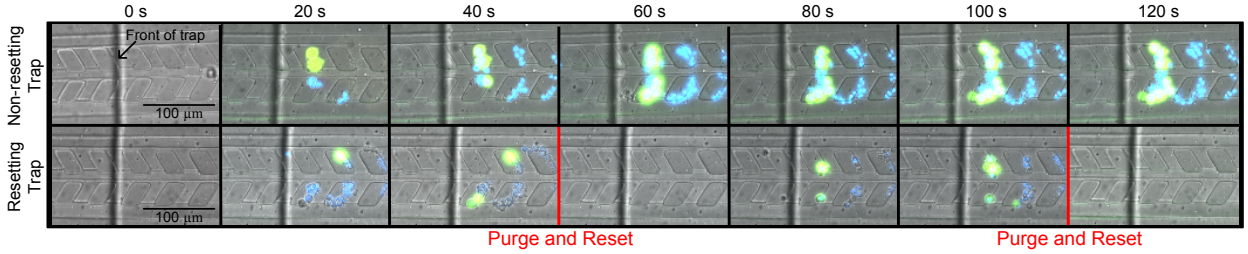

Figure 6. Comparison of a cell mixture flowing through a resetting trap and non-resetting trap mechanism. Each frame is a composite of bright field, blue fluorescence, and green fluorescence images. Target UC13 cells fluoresce green, background leukocytes fluoresce blue. The non-resetting trap functions properly for ~60 s, after which enough cells have accumulated in the cavities to clog the channel. The resetting trap is purged every 60 s and remains clean through multiple cycles.

Throughput

The prototype device contains 32 multiplexed channels that can process ~900,000 cells/hour. The overall throughput can be scaled by further parallelization with the only practical limit being the size of silicon wafer substrates used in photolithographic microfabrication. The total footprint for the 32-channel device is 4.5 cm^2 with only 0.77 cm^2 devoted to the cell traps and microchannels for multiplexing, equating to an area-normalized throughput of ~1200,000 cells/cm^2·hour. Therefore, scaling the resettable cell trap mechanism to cover the usable area of a standard 100 mm silicon wafer would result in a throughput exceeding $4 \cdot 10^7$ cells/hour. The throughput of the resettable cell trap mechanism compares favorably to other label-free cell separation techniques, exceeding the throughput of previous micropore filtration techniques by approximately a factor of 10 [**9**] [**19**] [**38**]. Ultra-fast cell separation methods with throughputs exceeding 10^7 cells/cm^2·hour can be achieved using inertial microfluidics, however these methods typically provide considerably lower enrichment [**39**] [**40**].

Application to the Separation of Circulating Tumor Cells

The separation of circulating tumor cells from peripheral whole blood is topic of significant current interest for physical cell separation technologies. The performance specifications required for this

application is extremely demanding in terms of both selectivity and throughput since the presence of as few as 5 CTCs in 7.5 ml of whole blood has been established as a prognostic marker in several types cancers [**41**]. Preprocessing steps such as CD45-based depletion of leukocytes can provide an initial CTC enrichment of ~100 [**42**]. Combining CD45-based depletion and the ~1000 fold enrichment provided by the resettable cell trap will result in a total enrichment on the order of 10^5, which would leave ~100 leukocytes per ml of blood, a quantity sufficiently small to allow for individual examination of cells by immunofluorescence to detect the CTCs. The throughput of the current 32-channel resettable cell trap mechanism is 450,000 cells per hour, which would enable 7.5 ml of whole blood to be processed in less than one hour following CD45 depletion. At this rate, identification and characterization would become the primary bottle-neck of the CTC enumeration process. Additional parallelization of this mechanism can potentially enable direct processing of whole blood.

Conclusion

We developed a resettable cell trap mechanism capable of simply and reliably adjusting the cross-section of a microfluidic channel to selectively capture cells based on size and deformability, and then subsequently release them for extraction and characterization. This capability addresses a long-standing challenge in filtration based cell separation systems of how to prevent clogging and adsorption in order to improve selectivity and enable the extraction of cells after separation. The resettable cell trap mechanism avoids clogging and adsorption by periodically clearing the filtration microstructures to allow sustained operation with high selectivity and throughput. Polystyrene spheres processed using this mechanism could be separated with <1 µm resolution. Rare UC13 cancer cells doped into a suspension of leukocytes can be enriched ~1800X with 90% yield despite the significant size overlap between the two cell types. Interestingly, leukocyte contamination in this filtration process was found to result primarily from non-specific adsorption, which can be mitigated using repeated filtration. The throughput of our prototype device consisting of 32 parallelized microchannels is 900,000 cells/hour, or ~1,200,000 cells/cm^2·hour on a per area basis, which exceed existing micropore filtration mechanisms by a factor of 20.

Acknowledgements

This work was supported by grants from Natural Science and Engineering Research Council of Canada, Canadian Institutes of Health Research, Vancouver Prostate Centre's Translational Research Initiative for

Accelerated Discovery and Development, and Engineers-in-Scrubs training program at UBC.

Materials and Methods

Sample Preparation

Cell separation studies were performed using leukocytes and UM-UC13 bladder cancer cells. Whole blood was drawn from healthy donors into 6 ml EDTA blood collection tubes. Whole blood is stained with Hoechst 33342 (Invitrogen) and diluted with PBS to a concentration of 2 million leukocytes per ml. UC13 bladder cancer cells were cultured in MEM solution with the addition of 10% (v/v) fetal bovine serum, 1% L-glutamine, 1% MEM Non-Essential Amino Acids, 1% Sodium Pyruvate (Invitrogen), and 1% Penicillin Streptomycin (Fisher Thermo Scientific, Waltham, MA), and incubated at 37°C in a humidified environment with 5% CO2. UC13 cancer cells were stained with calcein AM (Invitrogen) For separation studies, UC13 were doped into diluted whole blood. The mixed sample processed in each cell separation trial contained a minimum of 100 UC13. Each processed sample contained ~100,000 cells.

Fabrication

We fabricated the cell separation devices using standard multilayer soft lithography techniques [**30**]. Two master wafers were fabricated through photolithography to use as molds for the control and flow channels. To produce the control wafer, SU-8 3025 photoresist (Microchem Corp., Newton, MA) was spun on a silicon wafer at 3000 rpm for 30 seconds, exposed under a photomask (CAD/Art Services, Bandon, OR), and developed following the photoresist manufacturer's protocol. The flow wafer, comprising three separate feature heights, was produced by spinning and developing SU-8 3010, SU-8 3005, and SU-8 3025 for 30 seconds each at speeds of 2250 rpm, 3000 rpm, and 4000 rpm respectively. Each layer was aligned to the previous using a Canon PLA-501F mask aligner (Canon USA, San Jose, CA) before exposure. Rounded channels for microvalves were fabricated using SPR 220-7 photoresist (Rohm and Haas, Midland, MI) spun at 625 rpm for 50 seconds, then exposed and developed following the manufacturer's protocol.

Microfluidic devices for experiment were produced from the control and flow molds. To produce the flow layer, PDMS (Sylgard 184, Dow Corning, Midland, MI) was poured onto the flow wafer at a 5:1 ratio of base to crosslinker, degassed in a desiccator, and cured at 60°C for 1 hour. To produce the control layer, PDMS was spun on the control wafer at a 20:1 ratio of base to crosslinker at 1250 rpm for 60s and cured at 60°C for 1 hour. After curing the two layers were joined and left to diffusion bond overnight at 60°C. Fluidic ports and on-chip reservoirs were created using 0.5 mm OD and 6 mm OD punches,

respectively (Harris Unicore, Ted Pella Inc., Redding, CA). The punched devices were treated with plasma (Harrick Plasma, Ithaca, NY) and bonded to a clean glass slide. Prior to use, device channels were filled with a solution of 0.25% Pluronic F-127 and 5% BSA in MEM for surface passivation.

Experimental Apparatus

Fluids are loaded into the microfluidic device from 15 ml polypropylene reservoirs (BD Biosciences, Mississauga, Canada) fitted with custom machined caps that allowed the reservoirs to be pressurized from a pneumatic source. Fluids were delivered from these reservoirs via 0.5 mm ID flexible Tygon tubing (Cole-Parmer, Montreal, Canada) which connected to the microfluidic device through a 23 gauge stainless steel needle (New England Small Tube, Litchfield, NH). The pressure to actuate on-chip valves was controlled by on-off solenoid valves and controlled using a MSP430 microprocessor (Texas Instruments). A multi-channel variable pressure controller (MCFS-Flex, Fluigent, France) controlled the pressure of the sample and buffer reservoirs.

Experimental Characterization

Counting Cells

The performance of our cell separation mechanism was characterized by the percentage of UC13 cells captured by the cell traps (yield) and ratio of target cells to background cells in the output divided by the same ratio in the input (enrichment). These values were measured by counting the number of UC13 and leukocytes in the waste and collection reservoirs after separation. Individual cells were identified by their stains. After each cell separation test, cells in the reservoirs were left undisturbed for 10-15 minutes to allow the suspended cells to settle under gravity into a monolayer at the bottom of the reservoir. Microscopy was performed using an inverted microscope (Nikon Ti-E) and camera (QImaging, Surrey, BC, Canada). A manual Z-scan through the fluid in the reservoirs was first performed to check for unsettled cells. Next, tiled images of the waste and collection reservoirs were captured under both green and blue fluorescence using an automated translating stage and then stitched into a composite image (Microsoft Image Composite Editor). Finally, the UC13 cells in the waste and collection reservoirs, as well as the number of leukocytes in the collection outlet are manually counted. Sample composite images are shown in Supplemental Figure 1. Leukocytes in the waste outlet were too numerous to count directly. Instead, their quantity was estimated from the total number of UC13 processed and the UC13-leukocyte ratio in the original sample.

Measuring Cell Size

The size distribution of leukocytes and UC13 were determined by individually imaging at least 100 cells from each phenotype underneath a cover-slip using a calibrated and manually focused 60X objective lens. A watershed operation performed using ImageJ provided a measurement of cell area from which cell diameter was estimated. While cells imaged under a coverslip are known to appear larger than their true size in suspension [**43**], this technique is sufficient to assess the relative size of UC13 and leukocytes since any distortion caused by the slip will apply to both phenotypes.

Cell Deformability Measurement

The deformability of the cell types used in cell separation studies was measured using a microfluidic device developed previously by our group [**22**]. This device introduces single cells into a funnel shaped constriction where the pressure required to push the cell through the constriction is measured individually. To calibrate for differences in cell size, the cell is modeled as a liquid-filled sac where the cortical tension of the membrane is readout as the intrinsic stiffness of the cell. Figure 5B report the average and standard deviation of measurements of single cell cortical tension values, from at least 100 cells of each type.

Viability

The viability of captured cells was determined using a live/dead viability assay kit that tests cell membrane integrity. Briefly, UC13 cells were incubated in a 2 µM solution of calcein AM (Invitrogen) and a 1 µM solution of ethidium homodimer-1 (Invitrogen) for 30 minutes. The UC13 cells are then processed using the resettable cell trap device and collected them in an outlet reservoir, where they were counted using a fluorescence microscope. This process resulted in a decrease in viability of less than 0.5%.

References

[1] G. Vona et al., *Am J Pathol*, 2000, **156**, 1, 56-63.

[2] S. H. Seal, *Cancer*, 1964, **17**, 5, 637-642.

[3] C. G. Rao et al., *Int J Oncol*, 2005, **27**, 1, 49-57.

[4] B. van der Gun et al., *Carcinogenesis*, 2010, **31**, 11, 1913-1921.

[5] A. Chambers, A. Groom and I. MacDonald, *Nat Rev Cancer*, 2002, **2**, 563-572.

[6] S. Cross, YS. Jin, J. Rao and J. Gimzewski, *Nature Nanotechnology*, 2007, **2**, 12, 780-783.

[7] W. Xu et al., *PLOS ONE*, 2012, **7**, 10, e46609.

[8] M. Yamada, M. Nakashima and M. Seki, *Anal Chem*, 2004, **76**, 5464-5471.

[9] J. Davis et al., *Proc Natl Acad Sci USA*, 2006, **103**, 14779-14784.

[10] V. VanDelinder and A. Groisman, *Anal Chem*, 2007, **79**, 2023-2030.

[11] A. J. Mach, J. H. Kim, A. Arshi, SC. Hur and D. Di Carlo, *Lab Chip*, 2011, **11**, 17, 2827-2834.

[12] S. Choi, S. Song, C. Choi and JK. Park, *Anal Chem*, 2009, **81**, 1964-1968.

[13] F. Petersson, L. Aberg, AM. Sward-Nilsson and T. Laurell, *Anal Chem*, 2007, **79**, 5117-5123.

[14] P. RC. Gascoyne, *Anal Chem*, 2009, **81**, 8878-8885.

[15] J. Jung and KH. Han, *Appl Phys Lett*, 2008, **93**, 223902-223903.

[16] KH. Han and A. B. Frazier, *Lab Chip*, 2008, **8**, 1079-1086.

[17] D. Huh et al., *Anal Chem*, 2007, **79**, 4, 1369-1376.

[18] X. Chen, D. F. Cui, C. C. Liu and H. Li, *Sens Actuators B Chem*, 2008, **130**, 216-221.

[19] H. Mohamed, M. Murray, J. N. Turner and M. Caggana, *J Chromatogr A*, 2009, **1216**, 8289-8295.

[20] S. Zheng et al., *Biomed Microdevices*, 2011, **13**, 203-213.

[21] S. Zheng et al., *J Chromatogr A*, 2007, **1162**, 2, 154-161.

[22] Q. Guo, S. Park and H. Ma, *Lab Chip*, 2012, **12**, 15, 2687-2695.

[23] M. J. Rosenbluth, W. A. Lam and D. A. Fletcher, *Biophys Jl*, 2006, **90**, 2994-3003.

[24] R. M. Hochmuth, *J Biomech*, 2000, **33**, 1, 15-22.

[25] S. Quake, J. Marcus and C. Hansen, "Microfluidic Sieve Valves," 20080264863 A1, December 3, 2004.

[26] SB. Huang, MH. Wu and GB. Lee, *Sensors and Actuators B*, 2009, **142**, 1, 389-399.

[27] YH. Chang, CJ. Huang and GB. Lee, *Microfluid Nanofluid*, 2012, **12**, 1-4, 85-94.

[28] KH. Nam and D. T. Eddington, *JMEMS*, 2010, **19**, 2, 375-383.

[29] Q. Guo, S. Reiling, P. Rohrbach and H. Ma, *Lab on a Chip*, 2012, **12**, 1143-1140.

[30] M. A. Unger, HP. Chou, T. Thorsen, A. Scherer and S. R. Quake, *Science*, 2000, **288**, 113-116.

[31] Y. Xiang and D. A. LaVan, *Appl Phys Lett*, 2007, **90**, 13, 133901.

[32] T. Gerhardt, S. Woo and H. Ma, *Lab Chip*, 2011, **11**, 231-2737.

[33] L. Saias, J. Autebert, L. Malaquin and JL. Viovy, *Lab Chip*, 2011, **11**, 822-832.

[34] A. Jain and L. L. Munn, *PLoS One*, 2009, **4**, 9, e7104.

[35] S. Riethdorf et al., *Clin Cancer Res*, 2007, **13**, 920-928.

[36] A. Makino et al., *Biorheology*, 2007, **44**, 221-249.

[37] X. Chang and M. Gorbet, *Journal of Biomaterials Applications*, 2013, **28**, 3, 407-415.

[38] S. M. McFaul, B. K. Lin and H. Ma, *Lab Chip*, 2012, **12**, 2369-2376.

[39] S. S. Kuntaegowdanahalli, A. AS. Bhagat, G. Kumar and I. Papautsky, *Lab Chip*, 2009, **9**, 2973-2980.

[40] SC. Hur, A. J. Mach and D. Di Carlo, *Biomicrofluidics*, 2011, **5**, 0222061-10.

[41] M. Cristofanilli et al., *New England Journal of Medicine*, 2004, **351**, 8, 781-791.

[42] Z. Liu et al., *Journal of translational medicine*, 2011, **9**, 70,.

[43] G. W. Schmid-Schonbein, Y. Y. Shih and S. Chien, *Blood*, 1980, **56**, 866-875.